IJCSI International Journal of Computer Science Issues, Vol. 10, Issue 2, No 3, March 2013
ISSN (Print): 1694-0814 | ISSN (Online): 1694-0784
www.IJCSI.org

Human-Computer Interactive Fast Edge Matching of High Resolution Orthophotos

Jun Liu[1], Huaxing Bi[1], Jinzhao Zhu[1], Peilin Zhu[2], Xinjie Wang[2] and Guohua Li[3]

**[1] College of Soil and Water Conservation,
Beijing Forestry University,
Beijing 100083, P.R. China
[2] College of Forestry,
Beijing Forestry University,
Beijing 100083, P.R. China
[3] State Academy of Forestry Administration,
Beijing 100260, P.R. China**

Abstract

In the process of high resolution images orthorectification, an uneven distribution of ground control points in mountainous area results in the phenomenon of ground objects dislocation between orthophotos edges in the overlap area. Followed image mosaic, fusion and interpretation are seriously affected. High-resolution (2.5 m) panchromatic images with a 30% forward overlap of ALOS satellite were acquired over topography complication zones in Beijing mountainous area. After being ortho-rectified in Geomatica PCI 2012, odd or even serial numbered orthophotos on the same satellite track without edge overlapping were mosaiced and then experimental automatic matching tests between mosaic orthophotos and residual orthophotos were carried out in Automatic Registration of ENVI 4.8 to obtain empirical automatic matching parameters and guiding ground control points in the overlap areas. Finally, automatic edge matching operation was conducted by using parameters and guiding GCPs previously acquired. The results showed that mosaic alternate orthophotos in course line or lateral course lines shortened edge matching time effectively. In Automatic Registration module of ENVI 4.8, Search Window Size = 361, Moving Window Size = 19, Area Chip Size = 256 were empirical automatic matching parameters of ALOS panchromatic orthophotos. This method can accomplish high resolution orthophotos edge matching fast and accurately.

Keywords: *High Resolution Image, Orthophotos, Edge matching*

1. Introduction

High spatial resolution satellite image (referred to high resolution image) mostly refers to remote sensing image of spatial resolution within 5 m [1]. With the vigorous development in remote sensing, high resolution image is increasingly wide utilized in city planning, transportation, resources monitoring and many other trades and professions. Before being applied to practical utilization, high resolution images must be ortho-rectified to correct pixel displacement caused by factors such as atmospheric refraction, topographic relief and sensor errors. During the process, high accurate topographic map and DEM corresponding with image resolution are required. However, the existing large scale topographic maps of China were accomplished during 1980s and 1990s, which failed to keep pace with obvious changes of terrain characteristics in the past 20 years. In this sense collection Ground Control Points (GCPs) of even distribution and control of the total error were affected seriously, concretely manifesting in the following aspects: on the one hand, mountainous regions of non-updated topographic map could not be matched with the road system or landmark buildings in high resolution images, then the distribution of GCPs in the whole image failed to meet the requirement of uniformity and therefore orthorectification error occurred. On the other hand, due to the advance in image resolution, the whole study area usually could not be covered by a single image. While images with longitudinal overlap or lateral overlap being ortho-rectified by referring non-updated topographic map, ground objects dislocation and edge mismatching were found commonly between overlapping regions of images. Thus, images mosaics, fusion as well as the following interpretation got seriously affected.

To solve this problem, JiaWeiHua, CaiHong [2,3] successively adopted the LPS module of Erdas Imagine to ortho-rectify aerial images and Spot5 images of mining area. The results were satisfied both in overlapping the topographic map completely and in correcting edges dislocation of overlapping region. However, the limitation of this method lay in that the ephemeris information or Rational Polynomial Coefficient (RPC) corresponded with images was necessary to calculate geometric parameters when the sensor was taking photos. Then on the basis of selection GCPs and automatically measuring homonymy points, aerotriangulation could be conducted for ortho-rectifying images [4]. Dang Anrong etc. believed that excellent results could be obtained by using the AutoSync module of Erdas Imagine when images overlapping region was very small. Wu Lulu etc. used this module to accomplish automatic rectification and precise geometric correction between CBERS data and Landsat TM data [5]. Wan Lihong proposed a kind of fast precise registration method based on AutoSync in the processing of high resolution panchromatic images and color aviation photos. Those researches were mostly committed to rectification of high resolution images. However, few papers involving the solution of edge matching in longitudinal overlap and lateral overlap region in high resolution images could be found.

In this paper, panchromatic images with 2.5 m resolution taken by Japan ALOS satellite PRISM sensor are utilized as the experimental material to propose a kind of fast human-computer interaction edge matching method based on ENVI 4.8 Image Analysis Software. Empirical parameter setting of the related module is also put forward according to the experiment. The result shows that the proposed method is capable of matching dislocated edges of high resolution orthophotos overlapping regions which lays a sound foundation for precise mosaicing.

2. MATERIAL AND METHODOLOGY

2.1 Study area

The study area covers the whole Beijing city. Located in the northwest end of north China plain, Beijing embraces Taihang Mountain in the west, meets Yan Mountain in the north and faces Bohai Sea in the east. The mountains in the west of Beijing are referred to as the West Mountain, which belongs to Taihang Mountain range. The mountains in the north of Beijing are called Jundu Mountain, which belongs to Yan Mountain range. Beijing enjoys high elevation in west and north part and low elevation in east and south. The main topography is mountain land with an area of 10068.05km^2, which takes up 2/3 of the total area of Beijing. For the past 10 years, object feature such as infrastructures and road system in rural area has been improved obviously due to the new socialist countryside construction.

2.2. The experimental data

17 panchromatic images with a spatial resolution of 2.5 m which covered the whole region of Beijing were acquired by the PRISM sensor of Japan ALOS satellite. All the images were taken from September 26th 2009 to October 5th 2009 and delivered in 1B1 CEOS format, with cloud coverage of every single image less than 5%. The longitudinal overlap of images was about 30% of the total area in terms of size, while the lateral overlap was about 35%. 10 images when the satellite passed on 3 adjacent orbits were chosen to make a brief map based on the general covering contour to show the distribution of images and the overlap relationship among them in the study area (Figure 1). The background contour was the boundaries of Beijing administrative area. Number 2, 5, 6 and 9 of images had a large size of overlap with neighboring images.

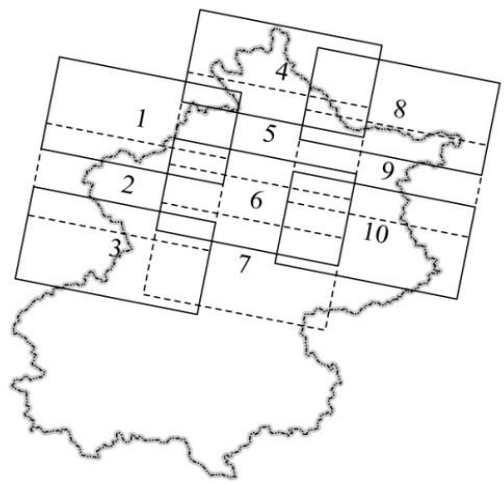

Fig 1. The distribution of 10 images covering contour of the study area

The Beijing topographic map with the scale of 1:10000 accomplished in the mid 1990s was used in the orthorectification. The scope of the map was confined to the Beijing administrative area. The coverage of edge images (Number 1, 2, 3, 4, 8, 9 and 10 of the images in Figure 1) exceeded the confine of the topographic map in different degrees. Taking image of number 1 in the upper left for example, the excess could be as much as 50%. The corresponding DEM with a spatial resolution of 30m for orthorectification was derived from ASTER GDEM data of International Scientific Data Service Platform. It has been verified that the 30m spatial resolution GDEM data is capable of meeting the accuracy requirement in the process of orthorectification [7].

2.3. Image orthorectification

Ortho-rectification method mainly includes strict physical model and general empirical model [8]. Collinear equation, as a representative of strict physical model, requires orbit parameters and attitude parameters of the sensor in order to obtain a high accuracy [9]. For the orthorectification of ALOS panchromatic data, OrthoEngine module of Geomatica 2012 developed by Canada PCI Company was utilized. Geomatica 2012 acquired flight trajectories and sensor parameters of common commercial satellites and supported strict satellite orbit models. Thus, orthorectification results had a high precision.

The 1B1 CEOS format of panchromatic images were firstly transformed to PCIDSK format (pix) with particular orbit parameter and rank information in OrthoEngine module. Images with PCIDSK format should not be clipped before orthorectification or the orbit parameter and rank information would be lost and the accuracy of correction result would be affected.

Collection GCPs in every image should follow the principle of even distribution and the Root Mean Square Error (RMSE) of GCPs should be confined to 1 pixel while keeping the number of them more than 20 [10].

However, in the process of orthorectification, excess of some regular shape images exceeding the actual range of topographic map together with the inhomogeneous distribution of GCPs resulted from inconspicuous geographic objects in mountainous areas caused common phenomena of ground object dislocations and edge mismatching in the overlap areas of different scenes edges. Images mentioned in the following discussion referred to these ortho-rectified images (namely orthophotos) with edge mismatching problem.

2.4 Automatic Registration algorithm

Human-computer interactive fast edge matching was implemented by using the function: Automatic Registration-Image to Image of ENVI 4.8 which was developed by Exelis Visual Information Solutions Company of the United States. The key algorithms of Automatic Registration were Moravec Operator or Förstner Operator.

Moravec Operator was developed by Hans P. Moravec in 1977, this operator utilized gray variance to extract salient points with properties of maximum or minimum gray variance in various directions [11, 12, 13]. Figure 2 shows four direction of Moravec operators.

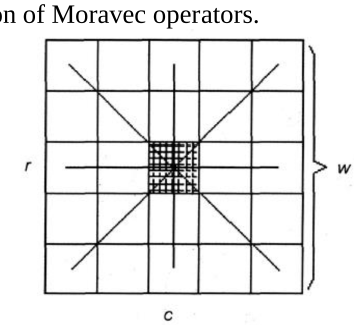

Fig 2. Four directions of Moravec operators

The algorithm can be formulated as follows,

$$V_1 = \sum_{i=-k}^{k-1} \left(g_{c+i,r} - g_{c+i+1,r} \right)^2$$

$$V_2 = \sum_{i=-k}^{k-1} \left(g_{c+i,r+i} - g_{c+i+1,r+i+1} \right)^2$$

$$V_3 = \sum_{i=-k}^{k-1} \left(g_{c,r+i} - g_{c,r+i+1} \right)^2$$

$$V_4 = \sum_{i=-k}^{k-1} \left(g_{c+i,r-i} - g_{c+i+1,r-i-1} \right)^2 \quad (1)$$

Where,

$$k = INT(w/2) \quad (2)$$

The minimum value is assigned to the salient point (c, r):

$$IV_{c,r} = \min\left(V_1, V_2, V_3, V_4\right) \quad (3)$$

Förstner Operator is a kind of location operator for extracting salient point being widely adopted in photogrammetry and computer vision. It was developed with the aim of creating a fast operator for the detection and precise location of interest points, corners and centers of circular image features with photogrammetric image matching applications in mind. In this algorithm, Robert grads of each pixel as well as gray covariance matrix based on an odd window taking pixel (c,r) as center are calculated to search the points of error ellipses which are as little as possible but close to circle as the interest points[12,13,14,15]. The procedures can be formulated as follows:

(1) Calculation Robert grads of each pixel

$$g_u = \frac{\delta g}{\delta u} = g_{i+1,j+1} - g_{i,j}$$

$$g_v = \frac{\delta g}{\delta v} = g_{i,j+1} - g_{i+1,j} \quad (4)$$

(2) Calculation gray covariance matrix in $l \times l$ pixels window

$$Q = N^{-1} = \begin{bmatrix} \sum g_u^2 & \sum g_u g_v \\ \sum g_v g_u & \sum g_v^2 \end{bmatrix}^{-1} \quad (5)$$

Where,

IJCSI International Journal of Computer Science Issues, Vol. 10, Issue 2, No 3, March 2013
ISSN (Print): 1694-0814 | ISSN (Online): 1694-0784
www.IJCSI.org

$$\sum g_u^2 = \sum_{i=c-k}^{c+k-1} \sum_{j=r-k}^{r+k-1} \left(g_{i+1,j+1} - g_{i,j} \right)^2$$
$$\sum g_v^2 = \sum_{i=c-k}^{c+k-1} \sum_{j=r-k}^{r+k-1} \left(g_{i,j+1} - g_{i+1,j} \right)^2$$
$$\sum g_u g_v = \sum_{i=c-k}^{c+k-1} \sum_{j=r-k}^{r+k-1} \left(g_{i+1,j+1} - g_{i,j} \right)\left(g_{i,j+1} - g_{i+1,j} \right) \quad (6)$$

(3) Calculation concerned values w and q

$$w = \frac{1}{trQ} = \frac{\det N}{trN}$$
$$q = \frac{4\det N}{(trN)^2} \quad (7)$$

Where,

$\det N$ represents the determinant of matrix N, trN represents the trace of matrix N.

(4) Determination of candidate points
An interest point is only precisely located when the given threshold values w_{min} and $q_{\min}$ are exceeded. Suitable parameters for threshold values can use empirical formula (8) as reference formula:

$$\left. \begin{array}{l} T_q = 0.5 \sim 0.75 \\ T_w = \begin{cases} f\bar{w} & (f = 0.5 \sim 2) \\ cw_c & (c = 5) \end{cases} \end{array} \right\} \quad (8)$$

Where $\bar{w}$ and w_c denote the mean and median value of the weight.
When $q > T_q$ and $w > T_w$, the pixel can be selected as a candidate point.

(5) Selection of extreme point
The weight w is set as a basis to select extreme point, the maximal candidate point is picked out within an appropriate window while the rest are abandoned.

Comparison between Moravec operator and Förstner operator has been studied in some experiments. The result showed that Moravec operator ran faster than Förstner operator while the accuracy of the latter was higher than the former [16, 17, 18].

2.5 Human-computer interactive fast edge matching

Moravec operator and Förstner operator were introduced into Automatic registration module of ENVI to search feature points in images. Then a window of certain size (a square subset of the image) scanned in the overlapping area of images to detect topographic feature points with identical or similar gray value in corresponding regions for matching. After generating a lot of matching points as well as some manual adjustment of RMSE, affine transformation or cubic polynomial transformation was employed to export corrected image. By this means, automatic registration was accomplished.

Human-computer interactive fast edge matching of high resolution orthophotos was based on Automatic registration module. 10 images in Figure 1 were taken for example, technique flow chart was shown in Fig 3.

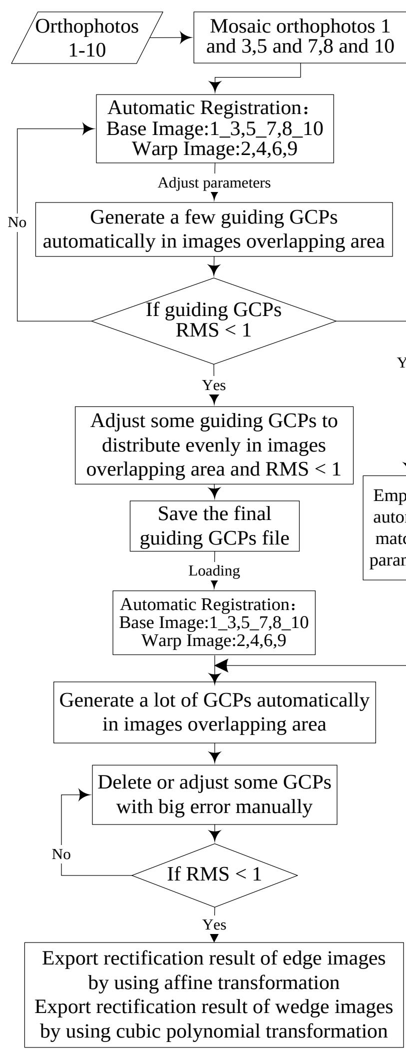

Fig 3. Fast edge matching flowchart of human-computer interaction

The method was achieved through the fast automatic collection of GCPs in the overlapping regions, manual adjustment of some GCPs and the automatic matching in the overlapping region. The main steps were shown below:

(1) The determination of base images with edge matching type -- initial mosaic of images in odd/even sequence
The determination of base images was generated by mosaicing orthophotos of odd or even sequence in the same satellite orbit or different orbit. No overlap region existed in these original mosaicked orthophotos. Selection of orthophotos in odd/even sequence was depended on the actual topographic scope they covered. Generally, original mosaic was conducted using orthophotos with large coverage rates. Take number 1 to number 10 orthophoto in figure 1 for example, the number 1 and 3, 5 and 7, 8 and 10 orthophotos were chosen in the 3 orbits for original mosaic respectively to obtain base images, namely 1_3,5_7,8_10. The rest orthophotos were called Warp Images.

After base images were determined, edge matching type could be divided into two categories according to edge overlap relationship between warp images and base images.

Wedge type: warp images were in the middle of the base image. There were two overlap regions between the warp image and the base image (upper and lower parts, or the left and the right parts), as was shown in figure 3 that the overlap relationship between number 6 orthophoto (single orthophoto) and image 5_7 (mosaicked orthophotos) or orbit B orthophotos and orbits A_C orthophotos.

Margin type: warp images stood on the upper or lower edge of the base image. There was only one overlap region between the warp image and the base image, just as the relationship between number 4 orthophoto (single orthophoto) and orthophoto 5_7 (mosaicked orthophoto), which was shown in figure 4.

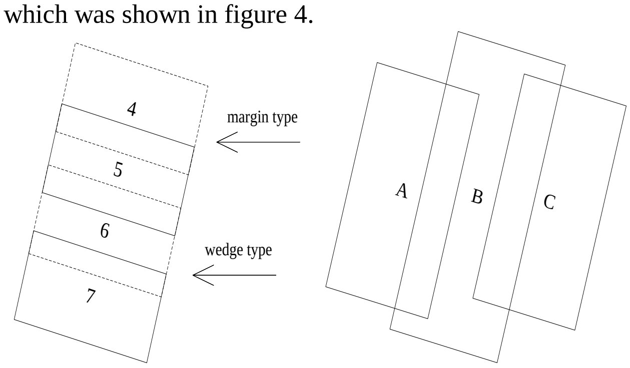

Fig 4. Types of orthophoto edge matching

(2) Determination of empirical automatic matching parameters and the automatic generation of seeded GCPs -- tentative edge automatic matching between warp images and base images.

With the Automatic Registration function, after setting the mosaicked orthophoto 5_7 as base image and number 6 orthophoto as warp image, the panel of Automatic Registration Parameters appeared. Setting with appropriate parameters led to the generation of mass GCPs with high precision which was the key point of precise edge matching. Each parameter in the Automatic Registration Parameters setting window was described in table 1 [11].

Table 1: The description of automatic registration parameters

Parameters	Description
Number Of Tie Points	Specify the number of tie points to generate, the default is 25.
Search Window Size	Specify the search window size, in square pixels. The search window is a defined subset of the image, within which the smaller moving window scans to find a topographic feature match for a tie point placement. The search window size can be any integer greater than or equal to 21, but it must be larger than the **Moving Window Size**. The default is 81.
Moving Window Size	Specify the moving window size, in square pixels. The moving window scans methodically in the image subset area defined by the Search Window Size, looking for matches to a topographic feature. The moving window size must be an odd integer. The smallest allowable value is 5. The default is 11.
Area Chip Size	Specify the image chip size to use to extract tie points. The default is 128 (128 x 128), which works best in most instances. The minimum setting is 64, and the maximum setting is 2048.
Minimum Correlation	Specify the minimum correlation coefficient required for a pair of conjugate points for candidate match. Any tie points with a correlation coefficient less than setting value would be removed. The default is 0.70.
Point Oversampling	Specify the number of tie points to collect from a single image chip. The default is 1.
Interest Operator	Specify the interest operator to identifying feature points. Moravec（by default）/Forstner
Moravec/Forstner	Moravec : Searches for gray scale value differences between one pixel and its adjacent pixels. The Moravec operator is typically faster than the Förnster operator. Forstner : Obtains and analyzes the gray scale gradient matrix between one pixel and its adjacent pixels. The Förnster operator is typically better for image matching than the Moravec operator.
Examine tie point before warping	Use this toggle button to indicate whether or not to allow the examination of tie points before warping the image. The default is Yes.

The number of tie points (namely GCPs in overlap region of orthophotos) was set to be 500. In order to ensure high matching accuracy, the minimum correlation coefficient was set to be 0.8. Förstner algorithm with the higher accuracy was chosen. Different combinations of the rest parameters were set for the tentative automatic matching between warp image and base image. It was better to get the RMSE of GCPs smaller than 2 pixels, the smaller the better. Combination with the low value of RMSE and short running time was chosen as the empirical automatic matching parameters. Automatic matching parameters at this time were determined to be the empirical automatic matching parameters of this spatial resolution which were also applicable to the automatic matching of rest orthophotos. After some manual adjustment, the generated GCPs could also be used as the seeded GCPs for generating large number of automatic matching GCPs. To ensure the precision of the final edge matching, seeded GCPs after adjustment should meet two demands:
①all of GCPs distribute evenly in overlap region.
②total error should be smaller than 1 pixel.

(3) The warp image and the base image edge rematching -- rectification and export

In this step the Automatic Registration function was utilized again. After setting the warp image and the base image, the guiding GCPs file was loaded for guiding the generation of mass GCPs. The number of GCPs generated this time was set to 4-10 times as many as the number of former tentative one according to the scope of the overlap region. Then empirical automatic matching parameters were filled in the panel of Automatic Registration Parameters. After operating large number of matching GCPs was generated in overlap region. The Degree parameter in the Ground Control Point Selection window was the degree of polynomial used for calculating the error. This parameter was set to 3 to get accurate RMS Error. The order according to errors of GCPs was able to be sorted by selecting Order Points by Error of Option in Image to Image GCP List window. Deleting some GCPs with bigger error as well as adjusting some GCPs manually were suggested to control RMS Error. It was acceptable that RMS Error was reduced smaller than 1 pixel.

When exporting the warp image, different rectification methods were adopted according to the alternative types of images edge matching. Cubic polynomial was suggested for wedge type images to ensure higher accuracy (number 6 orthophoto in figure 4), while affine transformation (RST) was for margin type images (number 4 orthophoto in figure 4). Serious geometric distortion occurred when cubic polynomial method was adopted for margin type images, since no GCPs were distributed in sites without overlap.

3. RESULTS AND ANALYSIS

RMS Error and operating time corresponding to different combinations of automatic matching parameters for the tentative matching were listed in Table 2, where the mosaicked orthophoto 5_7 was set as the base image, number 6 orthophoto was set as the warp image, and the initial Number Of Tie Points was 500.

The result showed that: the default combination (the 1st combination in Table 2) finished the automatic matching in minimal time, whereas the RMS Error （2.052813） exceeded 2 pixels. Manual adjustment to Search Window Size, Moving Window Size and Area Chip Size was able to confine RMS Error of GCPs within 2 pixels effectively. RMS Errors of GCPs according to the 5th, 8th, 10th, 12th, 14th and 17th combination were extremely closed to 1 pixel (RSM Error<1.2), among which the 10th combination （Search Window Size=961, Moving Window Size=31, Area Chip Size=128） had the minimum RMS Error of 1.109866 and the 5th combination Search Window Size=361, Moving Window Size=19, Area Chip Size=256）finished matching in minimal time (3′ 56″ 92 RMS=1.132772. In the case of setting initial Number of Tie Points with 500, there was no obvious effect on the number of GCPs actually generated when parameters were changed. With the increase of Area Chip Size value, the running time became longer obviously, however, the RMS Error was not controlled effectively.

Special attention was paid to combinations of parameters with RMS Error less than 1.2 pixels. After GCPs errors of these combinations were sorted by magnitude, they were able to be confined to 1 pixel rapidly by deleting or adjusting the first ten GCPs manually. RMS Error of automatic matching GCPs as well as corresponding running time were comprehensively considered, the parameter combination of Search Window Size=361, Moving Window Size=19, Area Chip Size=256 (the 5th combination of parameters in Table 2) was suggested to be the empirical parameter for automatic edge matching of these orthophotos.

Table 2 The operation results of different automatic edge matching parameter combination

Number of Parameter Combination	Initial number of GCP	Search Window Size	Moving Window Size	Area Chip Size	Number of GCP generated automatically	RMS Error	Running time
1	500	81	11	128	171	2.052813	56″57
2	500	81	11	256	168	1.352816	2′51″93
3	500	81	11	512	164	1.949267	11′37″17
4	500	361	19	128	175	1.935257	1′52″68
5	500	361	19	256	181	1.132772	3′56″92
6	500	361	19	512	172	1.202257	15′04″68
7	500	625	25	128	180	1.925621	4′43″09
8	500	625	25	256	183	1.149709	6′46″45
9	500	625	25	512	177	1.235704	15′37″09
10	500	961	31	128	187	1.109866	10′37″51
11	500	961	31	256	188	1.117683	12′45″76
12	500	961	31	512	183	1.162534	21′39″98
13	500	1296	37	128	177	2.726945	4′42″48
14	500	1296	37	256	177	1.153365	6′42″65
15	500	1296	37	512	172	1.328561	15′05″23
16	500	1849	43	128	176	3.037802	8′25″53
17	500	1849	43	256	171	1.193586	10′44″86
18	500	1849	43	512	164	1.210546	19′50″21
19 *	2000	361	19	256	910	1.080560	13′21″50
20 *	8000	361	19	256	2619	3.073721	48′33″61

Where the 19th combination was for mosaicked orthophoto 5_7 and number 6 orthophoto, the 20th combination was for orthophotos of orbit B and orthophotos of orbit A_C

RMS Error of GCPs generated by the 5th combination was able to be decreased to 0.981892 only by deletion of previous 3 GCPs with bigger error. GCPs with error adjusted were saved as the guiding GCPs file. Under the guidance of the guiding GCPs file and empirical automatic matching parameters, matching between mosaicked orthophoto 5_7 and number 6 orthophoto was conducted again. The result was also listed in Table 2 (the 19th combination). It was indicated that the guiding GCPs file together with empirical automatic matching parameters led to generate mass GCPs with high accuracy (RMS Error =1.080560) in less than 14 minutes. After sorting errors of GCPs by magnitude and deleting previous 9 with bigger error, RMS Error was dropped down to 0.996183 rapidly which already met the requirement of the principle that RMS Error should be smaller than 1 pixel. Number 6 orthophoto with mass matching GCPs in upper and lower parts was finally exported by cubic polynomial rectification. In order to check the actual effect of edge matching, the Swipe function and different stretch methods of PCI Focus window were utilized for visual inspection in overlap regions of orthophotos. A comparison of effects before and after edge matching was snapshot and shown in Figure 5. The result indicated that the matching degree of linear feature objects was perfect and high accurate edge matching was accomplished in overlap region between mosacked orthophoto 5_7 and number 6 orthophoto.

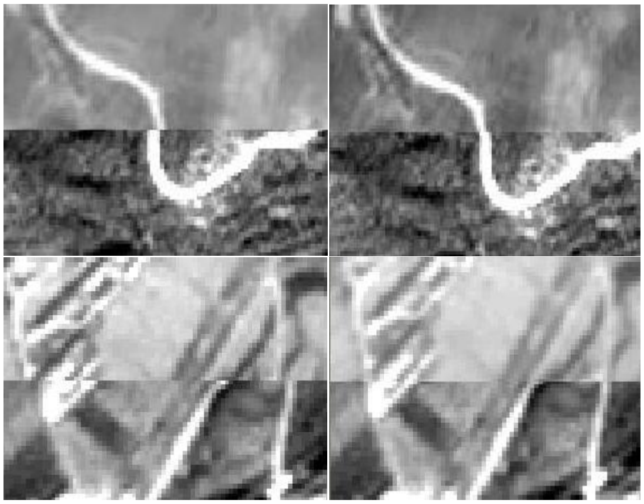

Fig5. A comparison of effects before and after edge matching
(Left: Before edge matching Right: After matching)

After the completion of edge matching among orthophotos in the same orbits, they were mosaicked into massive image, such as image of number A, B, and C shown in the right of Figure 4. After mosaicking massive image of number A and C, wedge type matching and empirical automatic matching parameters were adopted to deal with the final edge matching among massive images with lateral overlap in different orbits. The result showed that: 2619 GCPs were generated in the lateral overlap regions with RMS Error of 3.073721 in 48′ 33″ 61 (the 20th combination). After sorting GCPs error by magnitude and deleting previous 160 GCPs with larger error, RMS Error was decreased to 1.296625. Then manual adjustment to matching GCPs between base image and warp image was operated. However, it was found that there was a high probability that the ground objects of GCPs in base image was identical as those in warp image (the goodness of fit reached 92% according to previous 100 GCPs with larger error). While using the Predict button of Ground Control Points Selection Panel to predict the position of GCP selected in Image to Image GCP List to decrease error, the original matched GCPs lost their position. The RMS Error of GCPs was not reduced to 0.996719 until previous 793 GCPs with larger error were deleted. However, after doing these numerous deletions, the distribution of GCPs in the overlap regions was no longer even. This suggested that RMS Error had a tendency of being stable after deleting previous 160 GCPs with errors sorted by magnitude. Several reasons may account for this phenomenon: (1) changes of minor distortion in shape occurred since inappropriate preserving method of papery topographic map such as being moistened. These changes caused some errors during the process of scanning papery topographic map to electronic topographic map. (2) DEM adopted in the orthorectification process was GDEM with 30m sample interval, whose accuracy was far lower than panchromatic images with 2.5m resolution obtained by PRISM sensor of ALOS. This kind of mismatching in resolution together with uneven distribution of GCPs in mountainous regions led to larger error in these regions of orthophotos. Although original dislocated ground objects were matched perfectly by corresponding GCPS generated by Automatic Registration, larger errors of these GCPs in mountainous areas were not able to be reduced effectively.

4. Conclusion

(1) Human- computer interactive edge matching of high resolution orthophotos based on ENVI is able to solve the problem of edge mismatching in overlap regions of orthophotos caused by uneven distribution of GCPs rapidly and accurately.

(2) Mosaic of alternate orthophotos in course line or lateral course lines without overlapping can effectively decrease times of edge matching, save time, reduce error transmission among orthophotos and ensure the accuracy of edge matching in overlap regions. Consideration to accuracy and running time, the automatic matching parameters combination of Search Window Size=361, Moving Window Size=19, Area Chip Size =256 is selected as the first choice of empirical automatic matching parameters for ALOS panchromatic images with 2.5m resolution. These empirical automatic matching parameters can also be utilized as reference matching parameters for automatic rectification of images with the same resolution.

(3) In the process of edge matching for orthophotos in different orbits with lateral overlapping, the final RMS Error of GCPs can be confined within 1.5 pixels accordingly to ensure accurate overlap of ground objects in overlap regions.

(4) Human-computer interactive edge matching of high resolution orthophotos based on ENVI fills up the blank of solving the problem of image edge matching without RPC parameters and lays a sound foundation for subsequent accurate mosaic, fusion and interpretation of images.

Acknowledgments
This paper was supported by programs cooperated by education ministry and province of Beijing Municipal Commission of Education under Grant No. 2009GJKY01.

References
[1] Seto Yoichi, Kodaira Takatoshi, T.Jiang, "The Development of High Spatial Resolution Remote Sensing", Infrared, Vol. 9, 1997, pp. 1-8.
[2] A.R.Dang et al, ERDAS IMAGINE Remote Sensing Image Processing Course, Beijing: Tsinghua University Press, 2010, pp. 527-528.
[3] W.H.Jia, Y.P.Lv, and Z.W.Zhang, "Making of Digital Orthophoto Map Based on ERDAS 8.7 LPS", Geomatics & Spatial Information Technology, Vol. 6, 2007, pp. 39-43.
[4] H.Cai, P.Liu, and J.B.Song. "Ortho rectification of Spot5 Satellite Image Based on ERDAS LPS for the Environmental Investigation of Mines", Mining Research and Develop, Vol. 31, No.1. 2011, pp. 64-66.
[5] L.L.Wu, X.Luo, Y.Zhang, "Geometric precision correction of medium-low resolution images", Journal of Beijing Forestry University, Vol. S1, 2008, pp.78-82.
[6] L.H.Wan, Y.L.Shi, W.N.Yang, "Research of Quick Image Registration Based on AutoSync", Surveying and Mapping ,Vol. 3, 2010, pp.103-105.
[7] Q.J.Mo, W.S.Luo, "Study on Ortho-rectification of Spot5 Remote Sensing Image by Using GDEM", Forest Resource Management ,Vol. 2, 2011, pp. 90-92.

[8] Y.S.Zhang, D.C.Gong, Application of High Resolution Remote Sensing Satellites, Beijing: Science Press,2004, pp. 152-153.
[9] Q.Z.Luan, H.P.Liu, and Z.Q. Xiao, "Comparison between Algorithms of Ortho-rectification for Remote Sensing Images", Remote Sensing Technology and Application, Vol. 22, No. 6, 2007, pp. 743-747.
[10] W.J.Zhao et al, PCI Image Processing Course, Beijing: China Environmental Science Press,2007, pp. 324-325.
[11] H. P. Moravec, "Towards Automatic Visual Obstacle Avoidance". Proc. 5th International Joint Conference on Artificial Intelligence, 1977, pp. 584.
[12] Y.L.Guan, H.J.Zhang, and X.M.Liu, "Discussion on Interest Operators for Extracting Point-liked Features", Journal of East China Institute of Technology, Vol. 130, No. 1, 2007, pp.43-46.
[13] H.C.Chien, "On the evaluation of interest point detectors algorithm by using satellite images", M.S. thesis, Department of Civil and Environmental Engineering and Geodetic Science, The Ohio State University, Columbus, U.S.A.2010, pp.9-10.
[14] Förstner, W, and Gülch, "A Fast Operator for Detection and Precise Location of Distinct Points, Corners and Centres of Circular Features", Intercommission Workshop, 1987, June
[15] I. Jazayeri, C.S, "Fraser. Interest Operators in Close-range Object Reconstruction", The International Archives of the Photogrammetry, Remote Sensing and Spatial Information Sciences, Vol. XXXVII, Part B5, 2008.
[16] M. Trajkovic, and M. Hedley, "Fast Corner Detection. Image and Vision Computing", Vol. 16, No. 2, 1998, pp.75-87.
[17] C. Schmid, and R. Mohr, C. "Bauckhage. Comparing and Evaluating Interesting Points", International Conference on Computer Vision, 1998, pp. 230-235.
[18] F. Mohanna, and F. Mokhtarian, "Performance Evaluation of Corner Detection Algorithms under Similarity and Affine Transforms", BMVC, 2001.
[19] S.B.Deng, ENVI Remote Sensing Image Processing Method, Beijing: Science Press, 2010, pp 84-86.

Jun Liu, is a Ph.D. student in College of Soil and Water Conservation, Beijing Forestry University, China. He now focuses on forest remote sensing.

Huaxing Bi, PH.D., professor, corresponding author, supervisor in College of Soil and Water Conservation, Beijing Forestry University, China. His research interests include soil & water conservation and forest remote sensing.

Jinzhao Zhu, PH.D., professor, supervisor in College of Soil and Water Conservation, Beijing Forestry University, China. His research focuses on soil and water conservation.